LAWRENCE
LIVERMORE
NATIONAL
LABORATORY

UCRL-JRNL-237040

# Keck Observations of the 2002-2003 Jovian Ring Plane Crossing

I. de Pater, M. R. Showalter, B. A. Macintosh

December 6, 2007

Icarus

## Disclaimer

# Keck Observations of the 2002–2003 Jovian Ring Plane Crossing

Imke de Pater[1], Mark R. Showalter[2], and Bruce Macintosh[3]

1. Astronomy Department, 601 Campbell Hall
University of California, Berkeley, CA 94720

2. SETI Institute; 515 North Whisman Road
Mountain View, CA 94043

3. Lawrence Livermore National Laboratory
Livermore, CA 94550 USA

31 pages, 1 Table & 8 Figures (all in color)

Submitted to *ICARUS* 20 June 2007
revised manuscript: 11 November 2007

November 10, 2007

Running title: Keck Observations of the Jovian ring 2002–2003

**Editorial correspondence to:**
Imke de Pater
Department of Astronomy
601 Campbell Hall, University of California
Berkeley, CA 94720
phone: 510-642-1947
FAX: 510-642-3411
E-mail: imke@berkeley.edu

**Abstract**

We present new observations of Jupiter's ring system at a wavelength of 2.2 $\mu$m obtained with the 10-m W. M. Keck telescopes on three nights during a ring plane crossing: UT 19 December 2002, and 22 and 26 January 2003. We used conventional imaging, plus adaptive optics on the last night. Here we present detailed radial profiles of the main ring, halo and gossamer rings, and interpret the data together with information extracted from radio observations of Jupiter's synchrotron radiation. The main ring is confined to a 800-km-wide annulus between 128,200 and 129,000 km, with a $\sim$ 5000 km extension on the inside. The normal optical depth is $8 \times 10^{-6}$, 15% of which is provided by bodies with radii $a \gtrsim 5$ cm. These bodies are as red as Metis. Half the optical depth, $\tau \approx 4 \times 10^{-6}$, is attributed to micron-sized dust, and the remaining $\tau \approx 3 \times 10^{-6}$ to grains tens to hundreds of $\mu$m in size. The inward extension consists of micron-sized ($a \lesssim 10$ $\mu$m ) dust, which probably migrates inward under Poynting-Robertson drag. The inner limit of this extension falls near the 3:2 Lorentz resonance (at orbital radius $r = 122,400$ km), and coincides with the outer limit of the halo. The gossamer rings appear to be radially confined, rather than broad sheets of material. The Amalthea ring is triangularly shaped, with a steep outer dropoff over $\sim$5000 km, extending a few 1000 km beyond the orbit of Amalthea, and a more gradual inner dropoff over 15,000–20,000 km. The inner edge is near the location of the synchronous orbit. The optical depth in the Amalthea ring is $\sim 5 \times 10^{-7}$, up to 20% of which is comprised of macroscopic material. The optical depth in the Thebe ring is a factor of 3 smaller.

Keywords: PLANETARY RINGS, JUPITER, DUST

## 1. Introduction

Hints of the existence of Jupiter's ring system were first obtained in 1974, when Pioneer 11 detected "drop-outs" in the measurements of charged particle data (van Allen et al. 1975; Fillius et al. 1975). The nature of the system became much clearer in 1979, when Voyagers 1 and 2 obtained the first images of Jupiter's rings (Smith et al. 1979a, 1979b). Since that time several other spacecraft—Galileo, Cassini and New Horizons—have imaged the rings under a variety of viewing geometries, and both the 10-m Keck and 2.5-m Hubble Space Telescope (HST) took images while the rings were "edge-on", i.e., during a ring plane crossing or "RPX" (Showalter et al. 1985, 1987; Ockert-Bell et al. 1999; de Pater et al. 1999—hereafter dP99; Throop et al. 2004; Wong et al. 2006; Showalter et al. 2007b—hereafter S07).

The Voyager data showed the Jovian ring to be much brighter in forward- than backscattered light, suggestive of a large population of (sub)micron-sized dust. These observations also revealed several distinct components (Burns et al. 1984; Showalter et al. 1985, 1987): a *main ring* $\sim 7000$ km wide, with an abrupt outer boundary at 129,100 or $1.81 R_J$, where the Jovian radius $R_J = 71,398$ km. A more gradual inner boundary at $\sim 123{,}000$ km ($1.72\ R_J$), and a normal optical depth $\tau \approx$ a few $\times\ 10^{-6}$. Interior to the main ring lies the *halo*, which consists of a radially confined torus of faint material, with an inner boundary at $\sim 100,000$ km ($1.4\ R_J$) and $\tau \approx 10^{-6}$. The halo's full vertical thickness was measured to be $\sim 20,000$ km. The third component of the ring system is the extremely tenuous *gossamer ring* system ($\tau \sim 10^{-7}$), which extends from the main ring outward to $\sim 260,000$ km ($3.6\ R_J$), well beyond Thebe's orbit (Ockert-Bell et al. 1999).

As indicated by the optical depths given above, the Jovian ring system is extremely faint. Its precise structure and the nature of the ring particles are therefore challenging to measure. Observations in forward-scattered light are sensitive mainly to (sub)micron-sized grains, while measurements in backscattered light give information on larger grains and macroscopic bodies. Spectra of the rings and variations in intensity with phase angle provide information on the composition and size distribution of the particles, both of which are tied to the source of the rings. Throop et al. (2004) compiled such data on the main ring by combining Cassini, Galileo and ground-based observations, which together cover phase angles, $\alpha$, from $\ll 1^\circ$ to nearly $180^\circ$ and wavelengths from 0.4 to 4 $\mu$m. They concluded that the main ring is composed of a combination of small grains with a normal optical depth $\tau \approx 4.7 \times 10^{-6}$, and larger bodies at $\tau \approx 1.3 \times 10^{-6}$. They proposed a power law differential particle size distribution:

$$n(a)da \propto a^{-q} da \tag{1}$$

with $q \approx 2$ for particles with radii $a < 15$ $\mu$m, steepening to $q \approx 5$ for larger particles. The red color of the rings, however, which is very similar to that of the inner moons, could only be partially explained by light scattering off the ring's dust population. The authors, therefore, suggested that the larger particles must be distinctly red to explain the ring's color fully.

The gossamer rings are roughly an order of magnitude fainter than the main rings, and hence even less is known about their detailed radial structure. After the initial discovery by Voyager (Showalter et al. 1985), they were imaged in more detail in 1997 when the rings were viewed edge-on by Galileo and the Keck telescope. Showalter et al. (2007b) re-analyzed these data, together with new HST images. The Galileo data were taken in forward-scattered ($\alpha = 170 - 178^\circ$) and backscattered ($\alpha \sim 0$–$11^\circ$) light, at visible and near-infrared wavelengths. The Keck and HST observations are all in backscattered light at near-infrared (2.2 $\mu$m) and visible wavelengths, respectively. The ring is $\sim 3$ times brighter

in the infrared compared to the visible wavelength range, indicative of $q = 2.1$ in eq. 1 (SO7). The dependence on phase angle of all photometric data together also suggests $q$ to be between 2 and 2.5.

Because the lifetimes of micron-sized grains are brief ($\sim 10^3$–$10^5$ years for a 1 $\mu$m grain, Burns et al. 2004; hereafter B04) the rings must be young and continually replenished with material. The precise formation and destruction processes are, however, still unclear. Burns et al. (1999; hereafter B99) proposed that the rings originate from dust kicked off the moons Thebe, Amalthea, Adrastea and Metis by meteorite impacts, with subsequent orbital evolution inwards due to Poynting-Robertson (PR) drag. This model was developed to explain the vertical extent of the gossamer rings, with brighter top and bottom ridges, together with the observation that the outer edges of the two gossamer rings coincide with the orbits of Amalthea and Thebe. In this model, the particles stay on nearly circular orbits and conserve their orbital inclinations while they migrate inward. The vertical extent of the rings correspond to the orbital inclinations of Amalthea and Thebe.

In this paper we present results obtained during the 2002–2003 RPX with the Keck telescopes at 2.2 $\mu$m. We used both conventional imaging and adaptive optics techniques. These data provide new information on the radial and vertical structure of the rings, which helps define the various physical processes at work. In addition, we combine our results with published radio data (cf., de Pater et al. 1997) to obtain independent information on the population of larger "parent" bodies ( $\gtrsim$ 10 cm), which serve as the sources of the prevalent ring dust.

## 2. Observations and Results

### 2.1 Data Acquisition and Image Processing

We observed Jupiter's ring system with the 10-m W. M. Keck telescopes on Mauna Kea, Hawaii, in December 2002 and January 2003 when the rings were oriented nearly edge-on to Earth. A summary of the observations is given in Table 1. On UT 19 December 2002 and 22 January 2003 we obtained "conventional" images, using the facility's near-infrared camera NIRC (Matthews and Soifer 1994) on Keck 1. NIRC is equipped with a $256 \times 256$ pixel Santa Barbara Research Corporation InSb array, with a pixel size of $0.151''$, corresponding to 500 km at Jupiter. The observations were carried out with the $CH_4$ filter, which covers a wavelength range from 2.19 to 2.35 $\mu$m. Sunlight, usually reflected by Jupiter's thick cloud layers, is absorbed at this wavelength by methane and hydrogen gas in Jupiter's atmosphere, greatly reducing scattered light near the rings. The opening angle of the rings was $0.04^\circ$, so that the projected minor axis of the main ring is $0.05''$. The seeing was $\sim 0.7''$ on both nights so the rings are effectively seen edge-on. The dates of our observations were carefully selected to avoid interference by the Galilean satellites, as well as by Amalthea and Thebe. The images are, therefore, of much higher quality than those we obtained in 1997, where Amalthea and Thebe moved through the rings (dP99). The hexagonal Keck aperture causes six bright diffraction spikes to be scattered outward from Jupiter. We carefully timed the images so that these spikes, which rotate with respect to the sky as the telescope tracks, did not interfere with the rings.

All images were processed using standard near-infrared data reduction techniques, i.e., they were flat-fielded, sky-subtracted, and corrected for NIRC's known "bleeding" effect (Liu and Graham 2001). Bad pixels were replaced by the median of surrounding pixels. The absolute calibration of the images was set by observing HST IR standard stars (Persson et al. 1998). On 19 December we used SJ9134 and SJ9138, for which we adopted magnitudes of 11.596 and 10.982 in the $CH_4$ bands, respectively. On 22 January we used SJ9108 and SJ9118, with magnitudes of 11.336 and 11.261, respectively. The K-band flux density from

a zero-magnitude star is 660 Jy at this wavelength. With an average extinction coefficient $\tau = 0.1$, 1 count/sec corresponded to 0.170 $\mu$Jy at 1 airmass on both nights. Our calibration uncertainty is $\sim 3\%$.

On UT 26 January 2003 we used the adaptive optics (AO) system with NIRC2 on the Keck 2 telescope, a 1024 $\times$ 1024 Aladdin-3 InSb array. We used the K$'$ band (1.95–2.30 $\mu$m), with both the AO wide and narrow cameras, which have plate scales of 39.69 mas and 9.94 mas, repectively. These scales correspond to distances of 125 km and 31 km at Jupiter. We used Callisto for wavefront sensing. Initially, Callisto was positioned on top of Jupiter's main ring, but it moved outward from Jupiter during the night. (Fig. 1). When the satellite interfered with the ring, we observed the system in L$'$ band (3.43–4.13 $\mu$m). At this wavelength the Sun is less bright than at 2.1 $\mu$m, and Callisto could be imaged without dominating the background. Unfortunately, the background is much higher at this wavelength as well, so the ring was too faint to be detected (Wong et al. 2006). When Callisto had moved off the main ring and was moving through the gossamer rings, we observed the main ring in K$'$ band with the narrow camera. Once Callisto had moved through the Amalthea ring, we switched to the wide camera to image the entire ring system.

Like our conventional images, our AO images were processed using standard techniques. The calibration was defined by the IR standard star HD22686, which has a K-band magnitude of 7.185 (Elias et al. 1982). In the wide camera, 1 count/sec corresponds to 0.079 $\mu$Jy, and in the narrow camera 1 count/sec = 0.074 $\mu$Jy, both with an uncertainty $\lesssim 5\%$. Using a 6-th magnitude A0 star, which should result in similar AO performance to the brighter but slightly resolved Callisto, we determined a Strehl ratio of $\sim 25\%$ for the narrow camera images. (This is defined as the peak intensity of the point spread function or "PSF" divided by the peak intensity of the theoretical, diffraction-limited PSF.) The PSF's full width at half maximum (FWHM) was $\sim 0.08''$ in the wide camera and $0.05''$ in the narrow camera.

To compare our measurements with previous results and with physical models, we convert from units of Jy/pixel to the dimensionless ratio $I/F$. Here $I$ is the reflected intensity, and $\pi F$ is the incident solar flux density at Jupiter at the wavelength of observation. By this definition, $I/F = 1$ for a perfectly diffusing "Lambert" surface when viewed at normal incidence. We derived a factor of $1.31 \times 10^{-6}$ to convert units of $\mu$Jy/pixel on NIRC to $I/F$. On NIRC2, we used $6.63 \times 10^{-8}$ for the wide camera and $9.94 \times 10^{-7}$ for the narrow camera.

On each of the three nights, the images were carefully aligned and combined. The background in each combined image was fit based upon horizontal scans above and below the ring plane (outside the halo), and this background was subtracted from the images to get the best possible representation of the rings themselves (see e.g., dP99, de Pater et al. 2004a). The resulting images are shown in Fig. 2a,b.

### 2.2 Edge-on Views of the Rings

Our conventional images from 19 December 2002 and 22 January 2003, combined with those taken during the previous RPX in August 1997 (dP99) and October 1997 (S07, Wong et al. 2006), span phase angles between 1.2° and 11.0°. Because the data show no phase angle dependence (Wong et al. 2006, S07), we combined our 19 December 2002 and 22 January 2003 images to improve the signal-to-noise (SN) and overall quality (Fig. 2c). In this pseudo-color image, the main rings show up at left in red, with the halo in green-blue-purple around it. We adjust the contrast right of the dashed line to better show the gossamer rings; the Amalthea ring is light blue and the Thebe ring is violet. In the AO image (Fig. 2d), the main ring is red, halo is green, and the Amalthea ring is violet. Without

further processing, none of these images shows obvious radial structure in the rings. As we noted previously (dP99), some apparent radial variations in our 1997 image of the Thebe ring were artifacts caused by incomplete removal of the satellite.

### 2.3 "Onion-Peeling" and the Radial Distribution of the Rings

Because Jupiter's rings are optically thin, edge-on, and presumably cylindrically symmetric, we can invert the images by using an "onion-peel" deconvolution method (Showalter et al. 1987; dP99; de Pater et al. 2004a; Verbanac et al. 2005). We assume that each row in the image represents an edge-on radial profile of the rings. Starting from the outermost pixel in each row, we calculate the normal intensity of a narrow annulus that would produce the observed edge-on intensity. Then we subtract the expected contribution of that annulus to each interior pixel in that row and repeat. Because this process is akin to differentiation, it can only be applied successfully to images with a high SN. Our onion-peeled images are shown in Fig. 3. These images thus represent the true cross-sectional distribution of the rings, where all line-of-sight effects have been removed. Figure 3b shows the radial structure of the main ring as obtained from the conventional image. In Fig. 3c, the contrast has been changed to highlight the gossamer rings. The latter image clearly shows that the Amalthea ring is not a uniform band of material extending inward to the main ring, as predicted by the B99 model, but is mostly confined to a region just interior to the moon itself. The Thebe ring, being much fainter on the edge-on image, is barely visible in the onion-peeled image, although what little intensity can be seen is also concentrated near the tip. Although dP99 and S07 similarly suggested the Amalthea ring to be brightest near the tip, the data presented in this paper, having the highest SN of all data hitherto obtained in backscattered light, show this feature much more convincingly. Figure 3a shows the onion-peeled result from the AO image, which is focused on the main ring.

## 3. Image Analysis

### 3.1 Main Ring and Halo

*Edge-on Profiles*

Figure 4a shows edge-on profiles through the main ring and halo from conventional images (Fig. 2c). Intensity has been integrated vertically to produce "$VIF$":

$$VIF = \int_{z_{\min}}^{z_{\max}} \frac{I}{F} dz, \tag{2}$$

with $z$ normal to the rings. Because $I/F$ is dimensionless, $VIF$ is in units of meters. The fraction of the Jovian halo included in the scan depends on the vertical limits of the integration; several examples are shown. These scans are quite similar to those published by dP99 and Wong et al. (2006). The orbits of Metis and Adrastea, as well as the 3:2 and 2:1 Lorentz resonances are indicated by dotted vertical lines. In the broadest integral (dark blue), the halo is especially prominent between the two Lorentz resonances shown.

In Fig. 4b, we show profiles from the AO image obtained with the wide camera (cf. Fig. 2d). The two broader integrals (green and blue profiles) encompass both the halo and main ring. The narrower two (red and orange) contain the main ring only; before integration we subtracted the halo by taking scans above and below the main ring, just outside the PSF wings from the main ring. The profile from the 5000-km AO profile is $\sim 15\%$ less than that from the conventional profile (panel a), due to a loss of flux into the PSF's halo. The AO profiles show that the main ring is concentrated between $\sim 122,000$ and $\sim 128,000$

km, with a small spike at the very tip. Interior to the ring is a plateau at roughly half the intensity that extends inwards for at least 35,000 km; as is shown below, this is caused by viewing the annulus of the main ring edge-on. Figure 4c shows a scan through the AO image obtained with the narrow camera, which accentuates the narrow spike between the orbits of Adrastea and Metis.

*Radial Structure*

We have again used the onion peeling technique described in Section 2.3 to extract the radial profile of the ring system. Because the SN is higher on the vertically-integrated profiles (Fig. 4) than in single rows of an image (Fig. 2), the onion-peeled profiles show radial structure much more clearly. Figure 5a shows the inversion of the conventional profile (Fig. 4a), which encompasses both the main ring and halo. Again, these profiles are very similar to those presented by dP99[1]. They show a peak intensity near the orbit of Metis, with a decrease to almost zero on the outside and down to roughly half the intensity at $r \sim 122,000$ km, near the 3:2 resonance (122,400 km). The intensity then continues to drop to near zero at $\sim 100,000$ km, near the 2:1 resonance (101,200 km). The halo clearly appears to be confined by these Lorentz resonances, as has been discussed previously (Burns et al. 1985, B04).

Radial profiles extracted from the AO scans (Fig. 4b) are displayed in Fig. 5b. These profiles, having a spatial resolution $\sim 10$ times finer than those in panel (a), show that the main ring has a bright core $\sim 800$ km wide ($\sim 128,200$–129,000 km). Interior to this ring is a fainter sheet of material, with about half the intensity of the main ring, extending inward for $\sim 5000$ km. The intensity decreases gradually between 124,000 to 122,000 km to near zero at the 3:2 Lorentz resonance. Any material interior to 122,000 km is not confined to the ring plane and instead forms part of the halo.

Figure 5c shows the radial profile obtained by onion-peeling the edge-on profile from the AO narrow camera (from Fig. 4c). This profile was smoothed over 3 pixels ($0.03''<$ FWHM) radially to increase the SN. Superposed is the radial profile obtained by the Galileo spacecraft at visible wavelengths in backscattered light ($\alpha = 6°$; see B04). This profile was normalized to the Keck intensity in the inner extension of the ring. The Keck and Galileo profiles are remarkably similar. The double-humped structure between the orbits of Metis and Adrastea is notable; a similar ring profile was obtained recently by New Horizons (Showalter et al. 2007a). The gradual, stepwise decrease in intensity just outside the orbit of Adrastea is apparently caused by the spike in intensity seen in the full-resolution Galileo profile; our data support the Galileo observation that Adrastea is located in a gap in Jupiter's main ring.

*Vertical Structure*

Figure 6 shows north-south scans through the AO images of the main ring and halo. The profile through the main ring was taken at the tip of the ring (at 128,249 km), well outside the halo. The main ring is vertically unresolved in these data. The FWHM of $0.06''$ as measured in the narrow camera is very close to the diffraction limit of the telescope and corresponds to 188 km on the ring. Although in theory the diffraction limit is $\sim 0.045''$ at K′ band, our observations were conducted using Callisto for wavefront sensing, while the satellite was moving away from Jupiter. The anisoplanatic effect will naturally

[1] We note that the normal $I/F$ shown in dP99 is too low by a factor of 2 due to an error in the onion peeling program. This same error, unfortunately, propagated through in the Wong et al. (2006) Fig. 11.

degrade the resolution somewhat (see, e.g., de Pater et al. 2004b). The broader dashed line is a north-south scan through the tip of the main ring in the wide camera, and hence displays a broader profile (Section 2.1). The broadest profile, which peaks at about half the intensity of the main ring, is a north-south scan through both the main ring and halo in the wide camera, at a radial distance of $\sim 117,500$ km. The halo is clearly visible in this profile out to a distance of $\sim$ 4000 km. This comprises the bulk of the halo emission as observed via conventional techniques (Fig. 2, dP99).

### 3.2 Gossamer Rings

*Vertical Structure*

Vertical profiles through the gossamer rings are shown in Fig. 7. In panel (a) we show results from the conventional image (Fig. 2), through the Amalthea (blue) and Thebe (red) rings. The profiles were averaged radially over $\sim$ 7000 km (main part of Amalthea ring) and $\sim 35,000$ km (entire extent of the Thebe ring), respectively. Superposed are the B99 models, refined and presented in detail in S07, after convolution with the Keck PSF. This PSF was obtained by taking a north-south scan through the tip of the main ring, which, as expected, was similar to a gaussian profile with a FWHM of $\sim 0.8''$. The model intensities of the rings were scaled such that the peak intensity of the Amalthea ring matched the observed value. As shown, the models match the data quite well.

Figure 7b shows a vertical profile through the AO data of the Amalthea ring. The measured FWHM of $\sim$ 2600 km is consistent with the 2460 km thick ring expected based upon Amalthea's orbital inclination of 0.388° (B04), after convolution with the PSF (250 km FWHM). One can also distinguish the bright top and bottom morphology, as seen on Galileo images in forward scattered light (Ockert-Bell et al. 1999). The broad flanks of the profile reveal the Thebe ring, which indeed should have a width of $\sim$ 8300 km based upon Thebe's 1.07° orbital inclination. The observed intensity of the Thebe ring, however, is about half that expected from the model, and it does not reveal the edge brightening. A similar discrepancy was noted by S07 from Galileo data of the inner Thebe ring, which they attributed to a broader distribution of inclination angles of the ring particle orbits, which result from the numerous Lorentz resonances that are present throughout the Thebe ring region.

*Radial Structure of the Gossamer Rings*

Edge-on and radial (onion-peeled) profiles of the gossamer rings, as derived from the conventional image in Fig. 2, are shown in Fig. 8. We show profiles integrated vertically over 5000 km (red) and 9300 km (blue). Given the true widths of the rings, 2460 km for the Amalthea ring and 8290 km for the Thebe ring, the 5000 km profile would encompass the entire Amalthea ring and the 9300 km profile the Thebe ring (see Fig. 7a). All profiles were smoothed radially over 5 pixels, approximately equal to the FWHM of the PSF ($0.75''$ or 2500 km on Jupiter). In the edge-on profiles, the Amalthea ring shows a clear maximum near the tip of the ring, between 165,000 and 180,000 km, while the Thebe ring looks flatter, perhaps with slight variations in intensity.

The onion-peeled radial profile (red line, Fig. 8b) reveals a concentration of ring material just interior to and overlapping with the orbit of Amalthea. The ring shows a triangular-shaped profile, with a steep outer dropoff over $\sim$ 5000 km, extending a few thousand km beyond Amalthea's orbit. The inner dropoff spans 15,000–20,000 km, perhaps with a narrow ($\sim$ 3000 km wide) peak and a broader ($\sim$ 9000 km) inward extension. In forward-scattered images from Galileo, the ring was also concentrated just interior to Amalthea's orbit, but Showalter et al. (S07) found it to be only 10,000 km wide and associated with

a longitudinally-confined concentration of material in Amalthea's orbit. Since the Keck profile is the result of coadding numerous images, longitudinal variations would not be detectable. Interior to the peak, the ring's profile drops to an intensity level $\sim 30\%$ that of the peak, with what looks like a subtle minimum near the location of synchronous orbit $r_{\rm sync} = 160,250$ km.

The Thebe ring's radial profile is best represented by the 9300-km vertical integration (blue in Fig. 8b). Unfortunately, the profile is quite noisy. We see subtle evidence for a ∼12,000 km broad annulus interior to Thebe's orbit, perhaps reminiscent of the peak interior to Amalthea. A much sharper peak was seen in Galileo images (S07), although at a high phase angle. The discrepancy could be a particle size effect or more evidence for longitudinal clumping in the gossamer rings. However, more data will be needed to fully characterize this feature.

## 4. Discussion

The detailed radial and vertical structure of the rings provides constraints on formation and "sculpting" processes. In the following sections we discuss our results on the main ring/halo and gossamer rings, respectively.

### 4.1 Main Ring and Halo

Our Keck data show that the thin main ring is dominated by a bright annulus $\sim 800$ km wide. It is primarily confined between the orbits of Metis and Adrastea (Figs. 5b,c), but extends slightly outward beyond Adrastea. The annulus dips in brightness near its middle. These results are generally consistent with data from Galileo and New Horizons, but reveal the precision with which Keck can continue to monitor the Jovian ring from Earth in the absence of spacecraft. These structures remain unexplained. A small satellite was proposed to cause the central dip (Showalter et al. 1987), but our Keck data would have revealed moons 3–4 km in radius and New Horizons has recently set a limit of 0.5 km (Showalter et al. 2007a). Burns et al. (1985) note that Amalthea's 5:3 orbital resonance falls at 129,170 km and may play a role in confining the material orbiting outside Adrastea; however, this resonance is very weak so its role is uncertain.

Interior to Metis, the ring decreases in brightness to near zero at $r \sim 122,000$ km (Fig. 5b, red curve). However, vertically broader integrals show that the halo continues inward to $r \sim 100,000$ km, where it too seems to vanish (Figs. 3b and 5a). These boundaries are closely associated with the two strongest Lorentz resonances in the system, the 3:2 at 122,400 km and the 2:1 at 101,200 km. The high SN of our data set provides a dramatic illustration of the dynamical connection between halo structure and resonances. Our data also reveal that the inner edge of the main ring coincides with the 3:2 Lorentz resonance and onset of the halo. This suggests that the ∼5000 km broad sheet of material interior to the main ring annulus must be comprised entirely of micron-sized material, since only such small grains are influenced by the Lorentz resonances.

Two different models have been proposed for the formation of the main ring and halo. The first is the B99 model, which was briefly discussed in the introduction. In this model, dust is knocked off the various moons in the system, and subsequently evolves inwards under PR drag. The orbit inclination is conserved in this process, and the particles essentially stay on their near-circular orbits. Horanyi and Cravens (1996) have proposed an alternative model. They invoke a plasma drag force for the dust's inward migration, which should lead to substantial changes in the eccentricity of a grain's orbit. The large eccentricities would result in a concentration of particles in a thin disk that extends radially from $\sim 80,000$

km out to $\sim 140,000$ km. Both models agree that the small grains are charged, and that their orbital inclinations jump when they cross the 3:2 Lorentz resonance, producing the halo. However, we find no evidence for a thin disk that extends interior to the main ring or beyond the orbit of Adrastea, so our results strongly argue against Horanyi and Cravens (1996) model.

Although the high resolution radial profiles presented in Fig. 5c reveal a striking similarity between the 2.1 $\mu$m Keck and visual-light Galileo data, some small differences are apparent. Relative to the inward extension, the main ring annulus in the Keck data is $\sim 15\%$ brighter than in the Galileo profile (Fig. 5d). In addition, Keck's intensity maximum just outside the orbit of Metis may be slightly broader. Variations with time, longitude or wavelength are possible explanations; the Galileo data were taken 5–6 years before the Keck observations and at visual wavelengths. Photometry of the New Horizons data (also at visual wavelengths) may help to settle this question, although Showalter et al. (2007) have already noted an absence of large-scale longitudinal asymmetries. A wavelength effect is perhaps the most plausible explanation; it would indicate that the annulus is red, matching the color of all the inner Jovian moons (see below). This is consistent with the expectation that the annulus is composed primarily of the "parent bodies" that produce most of the ring's fine dust.

In the following we will derive the optical depth that can be attributed to these parent bodies ( $\gtrsim 5$ cm in radius), to micron-sized dust ( $\lesssim 5$ $\mu$m), and to intermediate grains tens to hundreds of $\mu$m in size. The observed $I/F$ is related to a ring's normal optical depth, $\tau$:

$$\frac{I}{F} \equiv \frac{1}{4}\tau\varpi P(\alpha), \tag{3}$$

with $\varpi$ the single scattering albedo and $P(\alpha)$ the phase function at phase angle, $\alpha$. The single scattering albedo is related to a particle's geometric albedo, $p$:

$$p = \frac{1}{4}\varpi P(0). \tag{4}$$

The optical depth in backscattered light is dominated by large material. The equivalent width, or radially integrated intensity, of the main profile in the visible light Galileo data (Fig. 5c) is equal to $E_w = 0.52$ m. If the particle geometric albedo, $p$, is the same as that of Metis, $p = 0.06$, then the cross sectional area $\sigma = 2\pi r E_w/p \approx 7000$ km$^2$. The material is spread over a width $W \approx 1100$ km, and hence the normal optical depth $\tau = \sigma/(2\pi r W) \approx 8 \times 10^{-6}$. This is the total cross section seen in backscattered light, which consists of both parent-sized and micron-sized material. Note that if $p$ is larger, the optical depth decreases in inverse proportion. As mentioned above, the inward extension of the main ring, at half the intensity of the annulus, must consist of micron-sized ( $\lesssim 10$ $\mu$m) dust. Becaue this dust is presumably produced in the main annulus, half the optical depth in the annulus can probably be attributed to micron-sized dust, and the other half to larger particles. However, this larger material includes both the parent bodies (cm–km in size) producing the dust, and also grains tens to hundreds of $\mu$m across.

We can estimate the fraction of parent bodies by using observations of Jupiter's synchrotron radiation. De Pater et al. (1997) show that 80–100% of the energetic electrons in Jupiter's radiation belts with pitch angles $< 70^\circ$ (i.e., those that pass through Jupiter's equatorial plane during their bounce motion along field lines) are absorbed when traversing Jupiter's main ring while diffusing inwards. An electron typically loses $\sim 3\rho a$ MeV when

going through a dust grain of radius $a$ (in cm) and density $\rho$ (g cm$^{-3}$) (de Pater and Goertz, 1990). Hence, to effectively stop 10–20 MeV electrons takes pebbles or rocks larger than several cm. These particles make up the parent bodies in the ring, and are the same bodies responsible for the observed drop-out in the *in situ* measurements of charged particles by Pioneer 11 (Van Allen et al. 1975; Fillius et al. 1975). Typically, 10–20 MeV electrons traverse the main ring with a width of $\sim$ 1000 km in about 6 days (de Pater, 1981). The bounce period is 1.3 seconds (de Pater, 1981), so they will cross the ring $\sim 8 \times 10^5$ times. With a 90% chance of absorption during this time, the optical depth $\tau \approx 1.1 \times 10^{-6}$. We therefore conclude that the optical depth of parent bodies in Jupiter's main ring constitutes approximately 15% of the total optical depth sensed in backscattered light (assuming $p \approx 0.06$). With half the opacity due to micron-sized dust, approximately 1/3 can be attributed to grains tens to hundreds of microns across. This is the material that may degrade the energy of relativistic (synchrotron radiating) electrons, as discussed by de Pater and Goertz (1990).

As stated earlier, the equivalent width of the main ring's annulus is 0.52 m in the Galileo profile. From the Keck profile we find 0.90 $\pm$ 0.05 m (after correction for light lost into the PSF halo, which was determined by convolving an unresolved ring with the PSF). Hence the annulus is $\sim$1.7 times brighter at 2.1 $\mu$m than at visual wavelengths. For the inward extension we find a ratio of $\sim$1.5. Hence the ring annulus is indeed $\sim$ 15% redder than its inward extension, as discussed above (Fig. 5d). From the radio observations we found that 15% of the total optical depth in the main ring annulus is comprised of parent bodies. If these bodies are as red as Metis, a satellite that is $\sim$3 times brighter at 2.1 $\mu$m than at visual wavelengths (dP99), the difference in color between the main ring annulus and inward extension can be accounted for.

Based upon our Keck, Galileo and (indirect) microwave observations we conclude that Jupiter's main ring consists of a collection of parent bodies with diameters over $\sim$ 10 cm, including Metis and Adrastea, with a normal optical depth $\tau \approx 1.1 \times 10^{-6}$. These bodies are concentrated between the orbits of Metis and Adrastea, are probably very dark ($p \approx 0.06$) and are as red as Metis. Dust grains tens–hundreds of $\mu$m across, produced via meteorite impacts on and collisions between the parent bodies (including Metis and Adrastea) add an optical depth of $\sim 3 \times 10^{-6}$. Micron-sized dust that migrates radially inwards due to PR drag totals $\sim 4 \times 10^{-6}$ in optical depth. The inward extension of the ring, and also the halo, are composed entirely of these tiniest dust grains.

### 4.2 Gossamer Rings

Figure 8b contains our most detailed radial profile of the gossamer rings in backscattered light. The SN (but not the spatial resolution) is approaching that of the best high-phase mosaic from Galileo (S07). As also noted by Showalter et al. (2007b), it is clear that the B99 model of grains migrating steadily inward under PR drag needs some revision. Although the vertical extent of the rings, with bright edges at the top and bottom, generally agrees with the B99 model, the rings clearly are not the uniform sheets of material that the model would predict. The Amalthea ring, in particular, has a bright peak just interior of the moon's orbit. That peak is quite broad, $\sim$ 20, 0000 in full radial extent. The same peak is seen in Galileo images, but is narrower, $\sim$ 10, 000 km wide. The change in this feature's radial width between the two images is puzzling. Our spatial resolution is $\sim$ 2300 (FWHM) km and therefore cannot explain an observed change in width from 10,000 km to 20,000 km. Our low-phase data set emphasizes the larger grains in the ring, whereas high-phase visual images from Galileo emphasize the finest dust. So if the Amalthea ring includes larger grains, then the data could indicate that such grains have a broader radial distribution. However, dynamical arguments would suggest the opposite—that larger

grains are less responsive to non-gravitational forces and should remain closer to their point of origin, whereas tiny grains would evolve more quickly.

The Galileo data showed the narrow peak along the north edge only, which revealed its origin as a population of material trapped in Amalthea's orbit, perhaps at the Lagrange points. Fig. 8b was constructed from an image comprised of coadding of data, which were taken over a total time span of 8.5 hours on two separate nights (Table 1). Because both nights were selected to ensure that Amalthea and Thebe would be out of the way, most of the images were obtained with the moons $> 90°$ away from the ring ansa. Thus, if the brightness peak represents an incomplete arc, then that arc must be quite extended in longitude, and cannot be closely confined to the 60° Lagrange points. It could, however, be material in "tadpole" orbits that librate between L4 and L5. Such a longitudinally extended feature could explain the difference in radial widths between the Galileo and Keck results.

We see a possible dip in brightness near the synchronous orbit location (160,250 km). Plasma drag drives electrically charged particles away from this location, so the presence of a brightness dip here is suggestive of interesting physics at work. (In the gossamer ring discovery paper, Showalter et al. 1985 reported a subtle enhancement at this location, but that now appears to be an artifact of the viewing geometry, related to their incorrect assumption that the ring was vertically thin.) However, the absence of material evolving outward from the orbit of Amalthea argues against a strong role for plasma drag in the ring. It is also possible that the dip, or minimum intensity on the inward slope of the triangular profile, occurs just by chance at an interesting location. Additional data are needed to fully address this question.

The ring profile extends a few thousand km beyond Amalthea's orbit; its outer edge is near the 4:3 orbital resonance with Thebe, which is at 183,000 km. Like Amalthea's 5:3 orbital resonance at 129,170 km, the Thebe resonance is likely relatively weak, and hence its role in confining the ring's outer edge is uncertain. Whether Amalthea, like Adrastea, might clear a gap in the ring is unknown. A potential gap should have a width that is the sum of the Amalthea's radial motion and $\sim$ 3–4 times its Hill sphere. The former is $2ae = 1160$ km, where $a$ is Amalthea's semimajor axis and $e$ is its eccentricity; this is illustrated by the gray bar surrounding Amalthea's orbit in Fig. 8. The latter is $\sim$ 900 km, for a sum of $\sim$ 2000 km. This is large enough to be only marginally detected in our data.

If we assume that the particle scattering properties in the gossamer rings are the same as in the main ring annulus, the optical depth scales linearly with the observed $I/F$, i.e., $\tau \approx 5 \times 10^{-7}$ in the Amalthea ring, and $\tau \approx 1.5 \times 10^{-7}$ in the Thebe ring. De Pater and Goertz (1990) postulated the presence of bodies $\gtrsim$ 5-cm in radius based upon radial diffusion model fits to the energetic electron flux as measured by the Pioneer spacecraft. The authors derived a typical life time of $\sim 10^7$ sec for energetic electrons against absorption throughout the 1.8–4 $R_J$ region, which translates to an optical depth $\tau \approx 10^{-8}$. If all this material would be concentrated in a $\sim 12,000$ km wide ring near Amalthea, the optical depth in that ring would be $\sim 10^{-7}$. The parent population in the Amalthea ring (not counting Amalthea itself) thus contributes at least several percent, but no more than 20%, to the total optical depth. Micrometeorite impacts on and collisions between these bodies, including Amalthea, produce the dust that makes the ring visible.

Our detection of the Thebe ring is a bit too marginal to say very much about it. An enhancement interior to the orbit of Thebe is suggested, but the profile is too noisy to draw a robust conclusion. The peak is quite strong in the Galileo high-phase data (Fig. 16b of S07), raising the question of why it was not seen more clearly in Keck data. As with Amalthea, our observations generally kept Thebe $> 90°$ away from the ring ansa. Perhaps further imaging will enable us to distinguish between variations in longitude, time or wavelength.

## 5. Summary and Conclusions

We have presented new results on Jupiter's faint ring system, obtained via conventional and adaptive optics imaging with the Keck telescopes during the 2002–2003 ring plane crossing. We derived radial profiles for the main and gossamer rings, and analyzed these together with previously published radio data of Jupiter's synchrotron radiation. Our infrared data confirm the Galileo visible light results in that the main portion (annulus) of the main ring is confined to $\sim 800$ km between 128,200 and 129,000 km, from the orbit of Metis to $\sim 100$ km outside the orbit of Adrastea. Adrastea itself clears a gap in the ring. About 15% of the total optical depth of $8 \times 10^{-6}$ (assuming a geometric albedo $p = 0.06$) in this main ring annulus, $\tau \approx 1.1 \times 10^{-6}$, can be attributed to parent bodies $\gtrsim$ 5-cm in radius, including Metis and Adrastea. This material must be as red as Metis to fully explain our observations. Grains tens–hundreds of $\mu$m across make up $\sim 3 \times 10^{-6}$ in optical depth, while half the total optical depth, $\sim 4 \times 10^{-6}$, is provided by micron-sized dust. Although these numbers are overall consistent with previous studies (e.g., Showalter et al. 1987; Throop et al. 2004), none of these earlier works could determine the separate fractions of parent material ($a \gtrsim 5$ cm) and micron-sized dust ($a \lesssim 5$ $\mu$m) in the particle population that makes up the main ring annulus and inward extension.

The $\sim 5000$ km broad extension interior to the main ring annulus is approximately half as bright as the annulus. By combining our data with dynamical arguments, we concluded that this extension consists predominantly of micron-sized dust, which, afer being produced via micrometeorite impacts on and collisions between parent bodies in the main annulus, migrates inwards under PR drag. The orbital inclinations of the dust grains are increased at the Lorentz 3:2 resonance, near 122,000 km, which marks the inner edge of the main ring and onset of the halo. The halo extends inwards until the 2:1 Lorentz resonance at $\sim 100,000$ km, where the orbital inclinations of the particles are kicked up again. While this merely reconfirms a model first proposed by Burns et al. (1985), the fine sensitivity of our data illustrates the association between the halo boundaries and the resonance locations better than has generally been seen before.

The Amalthea and Thebe rings are confined to regions just interior to their bounding satellites. The Amalthea ring reveals a triangular shape, $\sim$20,000 km wide at its base. On the inside this ring extends roughly to the orbit of synchronous rotation (160,250 km), while on the outside the rings extends beyond Amalthea's orbit, and ends near the 4:3 orbital resonance of Thebe (183,000 km). The normal optical depth is $\sim 5 \times 10^{-7}$ in the Amalthea ring, and three times less in the Thebe ring. If all parent-sized bodies detected (indirectly) via microwave obervations in the gossamer ring region are distributed in $\sim$12,000 km wide rings near the orbits of Amalthea and Thebe, roughly 10% of the rings' optical depths would be comprised of these bodies ( $\gtrsim$ 5-cm radius).

Based upon the combined satellite, groundbased infrared and visible (HST) data, as well as observations of Jupiter's synchrotron radiation and *in situ* measurements of the charged particle data, a picture of the rings begins to emerge that looks far more complicated than hitherto considered. The rings appear to consist of both parent bodies ( $\gtrsim$ 5-cm radius) and dust. The dust is transported radially inward by PR drag, while orbital and Lorentz resonances sculpt the ring's appearance. Amalthea's low bulk density of $0.86 \pm 0.1$ g cm$^{-3}$ (Anderson et al. 2005) suggests a high porosity (30–70%; unless it is mostly composed of water ice). Such a high porosity hints at a violent collisional history. Amalthea may have been re-assembled after a former larger body was completely disrupted in a collision, while a fraction of the fragments remained in independent orbits, i.e., formed a ring around the planet. Continued meteorite impacts on and collisions between these parent-sized bodies, including the moons, produce the dust which makes the ring visible. Metis, Adrastea and

other parent bodies in the main ring annulus have also been postulated to be the end product of a completely disrupted larger object (B04).

*Acknowledgements*

The data presented in this paper were obtained at the W. M. Keck Observatory, which is operated as a scientific partnership among the California Institute of Technology, the University of California and the National Aeronautics and Space Administration. The Observatory was made possible by the generous financial support of the W. M. Keck Foundation. This particular study was partially supported by the National Science Foundation and Technology Center for Adaptive Optics, managed by the University of California at Santa Cruz under cooperative agreement No. AST-9876783, and under the auspices of the U.S. Department of Energy by Lawrence Livermore National Laboratory under Contract DE-AC52-07NA27344. It was further suppported by NASA grant NAG5-13370.

The authors wish to recognize and acknowledge the very significant cultural role and reverence that the summit of Mauna Kea has always had within the indigenous Hawaiian community. We are most fortunate to have the opportunity to conduct observations from this Hawaiian volcano.

## References

Anderson, J. D., Johnson, T. V., Schubert, G., Asmar, S., Jacobson, R. A., Johnston, D., Lau, E. L., Lewis, G., Moore, W. B., Taylor, A., Thomas, P. C., Weinwurm, G., 2005. Amalthea's Density Is Less Than That of Water. Science 308, 1291-1293.

Burns, J. A., Showalter, M. R., and Morfill, G. E., 1984, The ethereal rings of Jupiter and Saturn, in Planetary rings, ed. R. Greenberg and A. Brahic, Univ. of Arizona Press, Tucson, Arizona, p. 200-272.

Burns, J. A., Schaffer, L. E., Greenberg, R. J., and Showalter, M. R., 1985. Lorentz resonances and the structure of the jovian ring. Nature, 316, 115-119.

Burns, J. A., Showalter, M. R., Hamilton, D. P., Nicholson, P. D., de Pater, I., Ockert-Bell, M. E., Thomas, P. C., 1999. The formation of Jupiter's faint rings. Science 284, 1146–1150. (B99)

Burns, J. A., Simonelli, D. P., Showalter, M. R., Hamilton, D. P., Porco, C. C., Throop, H., Esposito, L. W., 2004. Jupiter's ring-moon system. In *Jupiter: Planet, Satellites & Magnetosphere*, Eds. F. Bagenal, T. E. Dowling, and W. McKinnon, pp. 241-262. Cambridge, UK: Cambridge University Press. (B04)

de Pater, I., 1981: A comparison of radio data and model calculations of Jupiter's synchrotron radiation, I. The high energy electron distribution in Jupiter's inner magnetosphere, J. Geophys. Res. 86, 3397-3422.

de Pater, I., and Goertz, C. K., 1990, Radial Diffusion of Energetic Electrons and Jupiter's Synchrotron Radiation: I. Steady State Solution, J. Geophys. Res., 95, 39-50.

de Pater, I., Schulz, M., and Brecht, S. H., 1997. Synchrotron evidence for Amalthea's influence on Jupiter's electron radiation belt, J. Geoph. Res., 102, No. A10, 22,043 - 22,064.

ring system near Earth's 1997 ring plane crossing. Icarus, 138, 214-223. (dP99)

de Pater, I., Martin, S., and Showalter, M. R., 2004a. Keck Near-Infrared Observations of Saturn's E and G Rings during Earth's Ring Plane Crossing in August 1995. Icarus, 172, 446-454

de Pater, I., F. Marchis, B. A. Macintosh, H. G. Roe, D. Le Mignant, J. R. Graham, and A. G. Davies, 2004b. Keck AO observations of Io in and out of eclipse. Icarus, 169, 250-263.

Elias, J. H., Frogel, J. A., Matthews, K., and Neugebauer, G., 1982. Infrared standard stars. Astron. J. 87 1029-1034.

Fillius, R. W., McIlwain, C. E., and Mogro-Campero, A., 1975. Radiation Belts of Jupiter: a second look. Science, 188, 465-467.

Horanyi, M., and Cravens, T. E., 1996. The structure and dynamics of Jupiter's ring. Nature, 381, 293-295. (HC96)

Ip, W.-H., 1980. Discussion of the Pioneer 11 observations of the F ring of Saturn. Nature, 287, 126-128.

Liu, M. C. and Graham, M. C., 2001. Infrared surface brightness fluctuations of the coma elliptical galaxy NGC 4874 and the value of the Hubble Constant. Astrophys. J. Lett. 557, L31–L34.

Matthews, K., and Soifer, B. T., 1994. The near infared camera on the W. M. Keck Telescope. In Infrared Arrays in Astronomy: The Next Generation (I. S. McClean, Ed.), 239-246, Kluwer, Dordrecht.

Ockert-Bell, M. E., Burns, J. A., Dauber, I. J., Thomas, P. C., Veverka, J., Belton, M. J. S., and Klaasen, K. P., 1999. The structure of the jovian ring system as revealed by the Galileo imaging experiment. Icarus, 138, 188-213.

Persson, S. E., Murphy, D. C., Krzeminski, W., Roth, M., and Rieke, M. J., 1998. A New System of Faint Near-Infrared Standard Stars. Astron. J., 116, 2475-2488.

Showalter, M. R., Burns, J. A., Cuzzi, J. A., and Pollack, J. B., 1985, Discovery of Jupiter's gossamer ring, Nature, 316, 526-528

Showalter, M. R., Burns, J. A., Cuzzi, J. N., Pollack, J. B., 1987, Jupiter's ring system: new results on structure and particle properties, Icarus 69 458- 498

Showalter, M. R., Cheng, A.F., Weaver,H.A., Stern,S.A., Spencer,J.R., Throop,H.B., Birath,E.M., Rose,D., and Moore,J.M., 2007a. Clump detections and limits on moons in Jupiter's ring system. *Science* **318**, 232–234.

Showalter, M. R., de Pater, I., Verbanac, G., Hamilton, D. P., and Burns, J. A., 2007b. Properties and dynamics of Jupiter's gossamer rings from Galileo, Voyager, Hubble and Keck images. Icarus, submitted

Smith, B. A., et al. 1979a. The Jupiter system through the eyes of Voyager 1. *Science* **204**, 951–972.

Smith, B. A., et al. 1979b. The Galilean satellites and Jupiter: Voyager 2 Imaging Science results. *Science* **206**, 927–950.

Throop, H. B., Porco, C. C, West, R. A., Burns, J. A., Showalter, M. R., and Nicholson, P. D., 2004. The jovian rings: new results derived from Cassini, Galileo, Voyager and Earth-based observations. Icarus, 172, 59-77.

van Allen, J. A., Randall, B. A., Baker, D. N., Goertz, C. K.. Sentman, D. D., Thomsen, M. F., and Flindt, H. R., 1975. Pioneer 11 observations of energetic particles in the Jovian magnetosphere. Science, 188, 459-462.

Verbanac, G., I. de Pater, M. Showalter and J. J. Lissauer, 2005. Keck Infrared Observations of Saturn's Main Ring System during Earth's 1995 Ring Plane Crossing. Icarus, 174, 241-252.

Wong, M. H., de Pater, I., Showalter, M. R., Roe, H. G., Macintosh, B., and Verbanac, G., 2006. Groundbased near-infrared spectroscopy of Jupiter's ring and moons. Icarus, 185, 403-415.

**Figure Captions**

Fig. 1. Geometry of Jupiter and Callisto during the AO observations on UT 26 Jan. 2003. We started observations at 07:58 UT, in L′ band. Callisto was moving away from Jupiter. At 09:20 UT we switched to K′ band, and at 10:00 we switched from the narrow to the wide camera. We could continue to use Callisto for wavefront sensing until 13:20 UT. (Figure adapted from the PDS Planetary Rings Node Jupiter viewer at http://pds-rings.seti.org).

Fig. 2. Edge-on images of the jovian rings. Panels a) and b) show images obtained on UT 19 Dec. 2002 and 22 Jan. 2003, with the combined image in panel c). Panel d) shows the AO image from 26 Jan. 2003. The dashed white line indicates a change in color scale from the main ring to the gossamer rings.

Fig. 3. Onion-peeled images from the data in Fig. 2. The middle row (b) shows the onion-peeled result of the conventional image from Fig. 2c. Panel c shows the same image, with a color scale that emphasizes the gossamer rings. The top panel (a) shows the radial distribution as derived from the AO image in Fig. 2d.

Fig. 4. a) Radial scans through the conventional image from Fig. 2c. The scans were vertically integrated as indicated in the legend. The intensity scale on the left side is the vertically integrated flux density in $\mu$Jy/linear arcsecond, while the scale on the right shows the VIF (vertical integrated $I/F$) in meters. The orbits of Metis and Adrastea, as well as 3:2 and 2:1 Lorentz resonances are indicated by dotted vertical lines.

b) Vertically integrated scans through the AO image in Fig. 2d. The top curves are integrated over both the main ring and halo, while the bottom two curves show the main ring only.

c) Vertically integrated scan through the AO image obtained with the narrow camera (not shown in Fig. 2). Note the difference in distance scale with panel (b). This region highlights just the outer $\sim 10,000$ km of the ring.

Fig. 5. a) Radial profiles through the main ring and halo, obtained by onion-peeling the edge-on profles from the conventional image in Fig. 4a. The orbits of Metis and Adrastea, as well as 3:2 and 2:1 Lorentz resonances are indicated by dotted vertical lines.

b) Onion-peeled results from the AO scans in Fig. 4b. The upper profile shows the resulting radial profile for the edge-on scan that was vertically integrated over both the main ring and halo. The lower profile shows the result for just the main ring. The orbits of Metis and Adrastea, as well as the Lorentz 3:2 resonance, are indicated.

c) A high resolution radial profile of Jupiter's main ring, obtained by onion-peeling the edge-on profile from the AO narrow camera (Fig. 4c; integrated vertically over 100 km). The profile was smoothed radially over $0.03''$. Superposed is a visible light Galileo profile at low phase angles ($\sim 6°$; from Burns et al. 2006), normalized to the intensity of the Keck profile's inner extension of the main ring.

Fig. 6. Vertical profiles through the edge-on AO images from 26 Jan. 2003. Profiles of the main ring (at a jovicentric distance of 128,249 km) are shown through the image obtained with the wide camera (Fig. 2d; averaged radially over $0.12''$) and the narrow camera (averaged radially over $0.05''$. The latter profile was normalized in intensity to the wide camera profile. The broad profile shows both the main ring and halo (averaged over jovicentric distances between 115,000 and 120,000 km) as observed with the wide camera.

Fig. 7. a) Vertical profiles through the Amalthea ring (averaged radially over 170,940-177,600 km) and the Thebe ring (averaged radially over 186,480-221,556 km) from the

conventional edge-on image in Fig. 2c. Superposed are the B99 Amalthea and Thebe ring models from Showalter et al. (2007), convolved with the Keck PSF.

b) Vertical profile through the edge-on AO image (Fig. 2d) of the Amalthea ring, averaged over the entire length of the ring. The scan was smoothed over 3 pixels, or 0.12″. Superposed is S07's model, convolved with the Keck PSF.

Fig. 8. a) Edge-on profiles through the gossamer ring system, integrated vertically over $\sim$ 1330 km, 5000 km, and 9300 km, as indicated. These profiles were obtained from the conventional image in Fig. 2c. The orbits of Amalthea and Thebe are indicated by the dotted lines. These profiles were smoothed over 5 pixels radially (0.75″).

b) Onion-peeled radial profile through the gossamer ring system, integrated vertically over 5000 km and 9300 km (from panel a). The orbits of Amalthea and Thebe, as well as the location of synchronous rotation ($r_{\rm sync}$) are indicated. These profiles were smoothed over 5 pixels radially (0.75″).

**Table I**

**Summary of Observations**

| UT Date<br>Date: UT hr range | Camera | Filter<br>($\mu$m) | # Images | Tint[a]<br>(sec) | $\Delta$[b]<br>(AU) | $r$[c]<br>(AU) | $\phi$[d]<br>(°) | $B$[e]<br>(°) | Pixel<br>("/pix) | Pixel<br>(km/pix) |
|---|---|---|---|---|---|---|---|---|---|---|
| 2002 Dec. 19: 11:00–16:30 | NIRC | $CH_4$ (2.19-2.35 $\mu$m) | 107 | 5580 | 4.614 | 5.298 | 8.2° | 0.039° | 0.151 | 505 |
| 2003 Jan. 22: 07:30–10:30 | NIRC | $CH_4$ (2.19-2.35 $\mu$m) | 62 | 1780 | 4.345 | 5.309 | 2.3° | 0.042° | 0.151 | 476 |
| 2003 Jan. 26: 07:58–09:20 | NIRC2[f] | L' (3.43-4.13 $\mu$m)[g] | 72 | 648 | 4.334 | 5.310 | 1.5° | 0.051° | 0.01 | 31.24 |
| 2003 Jan. 26: 09:20–10:00 | NIRC2[f] | K' (1.95-2.30 $\mu$m) | 36 | 720 | 4.334 | 5.310 | 1.5° | 0.051° | 0.01 | 31.2 |
| 2003 Jan. 26: 10:45–13:20 | NIRC2[f] | K' (1.95-2.30 $\mu$m) | 60 | 1200 | 4.334 | 5.310 | 1.5° | 0.051° | 0.04 | 124.7 |

[a] Total integration time is given; integration time per image varied between 10 and 60 sec.

[b] Geocentric distance

[c] Heliocentric distance

[d] Solar phase angle

[e] Ring opening angle

[f] AO observations, using Callisto for wavefront sensing.

[g] Reported in Wong *et. al.* (2006).

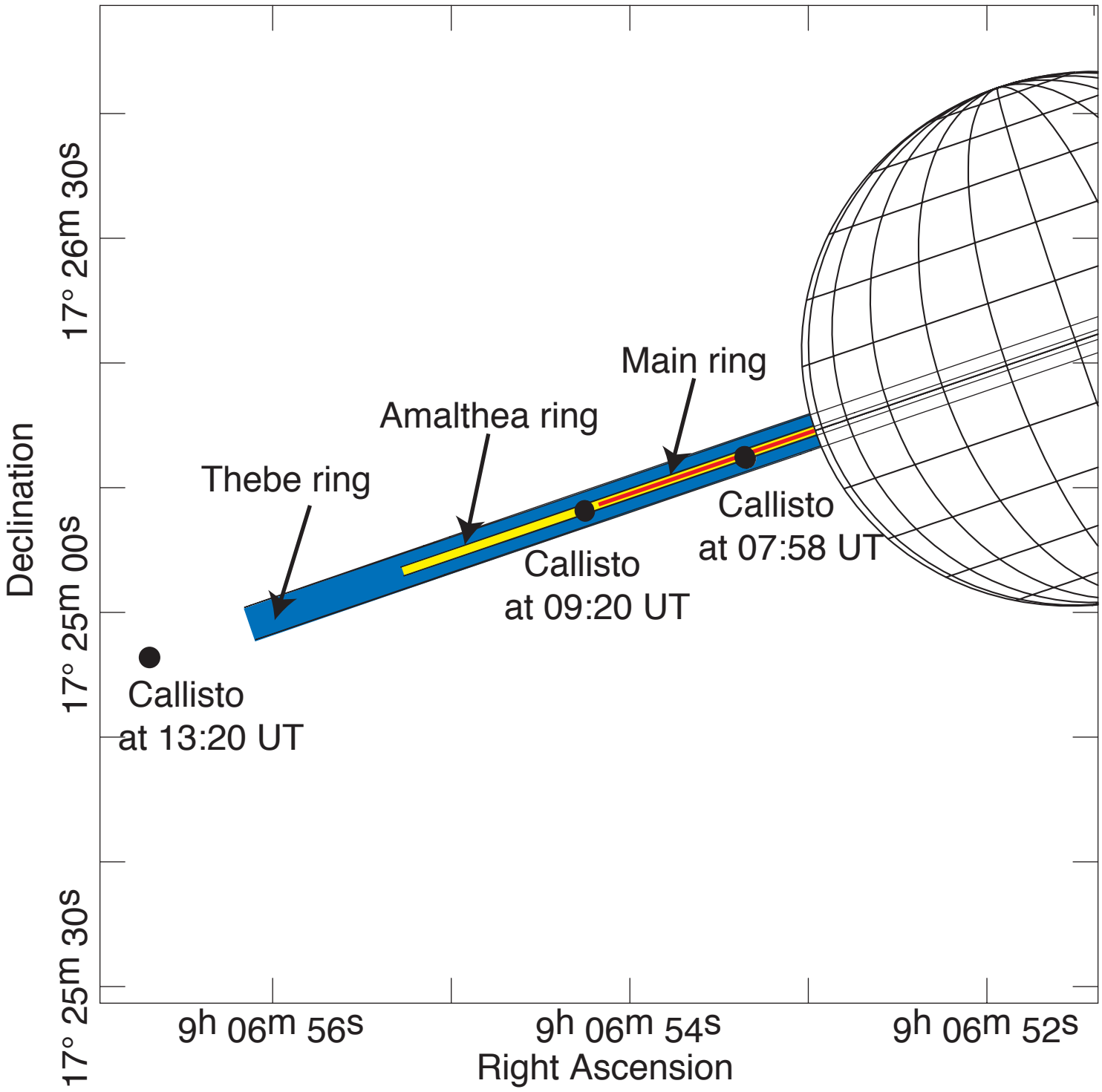
Main ring
Amalthea ring
Thebe ring
Callisto
at 07:58 UT
Callisto
at 09:20 UT
Callisto
at 13:20 UT
Declination
17° 26m 30s
17° 25m 00s
17° 25m 30s
9h 06m 56s
9h 06m 54s
9h 06m 52s
Right Ascension

Fig. 1

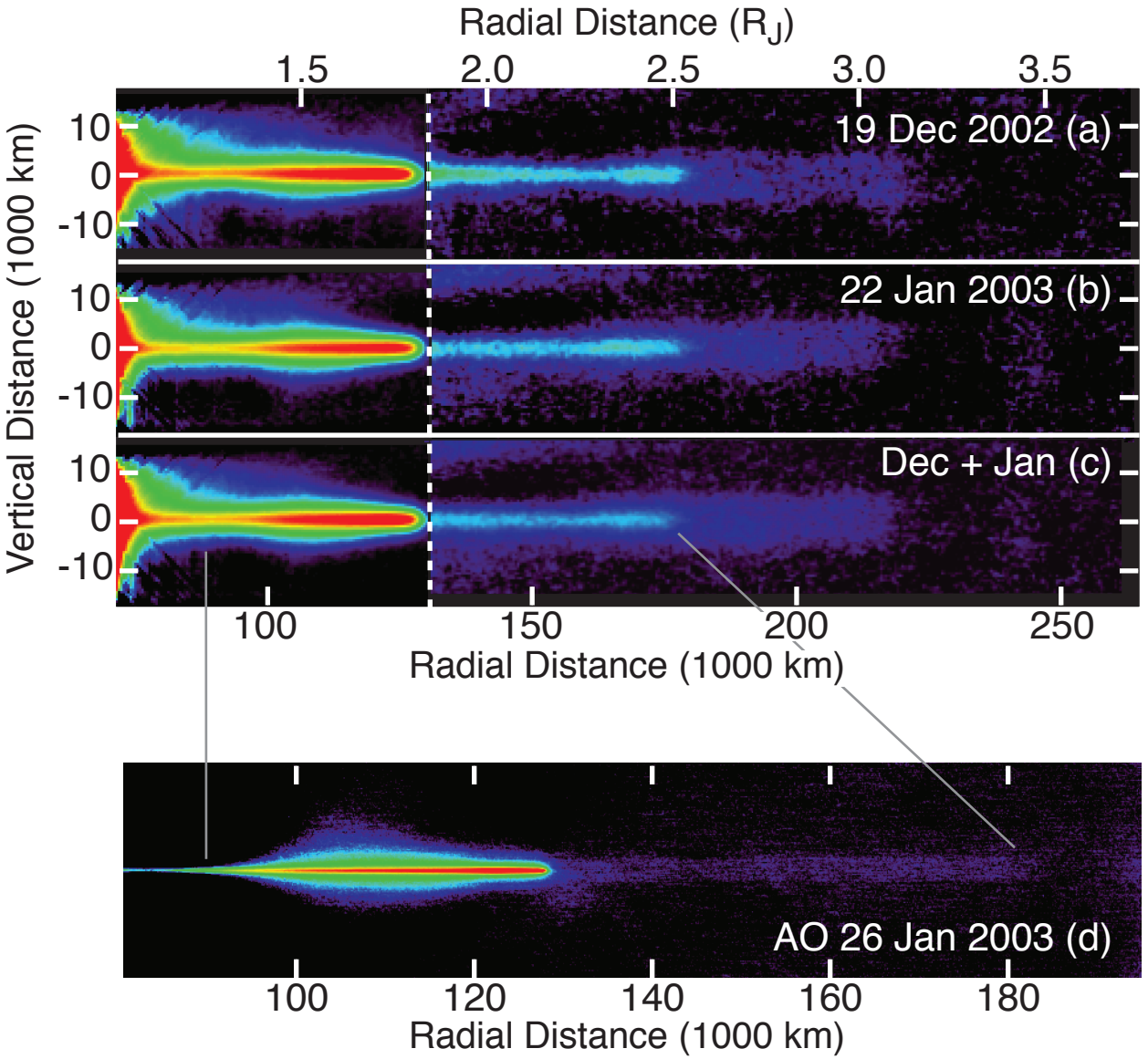
Radial Distance ($R_J$)
1.5
2.0
2.5
3.0
3.5
Vertical Distance (1000 km)
10
0
-10
19 Dec 2002 (a)
22 Jan 2003 (b)
Dec + Jan (c)
100
150
200
250
Radial Distance (1000 km)
AO 26 Jan 2003 (d)
100
120
140
160
180
Radial Distance (1000 km)

Fig. 2

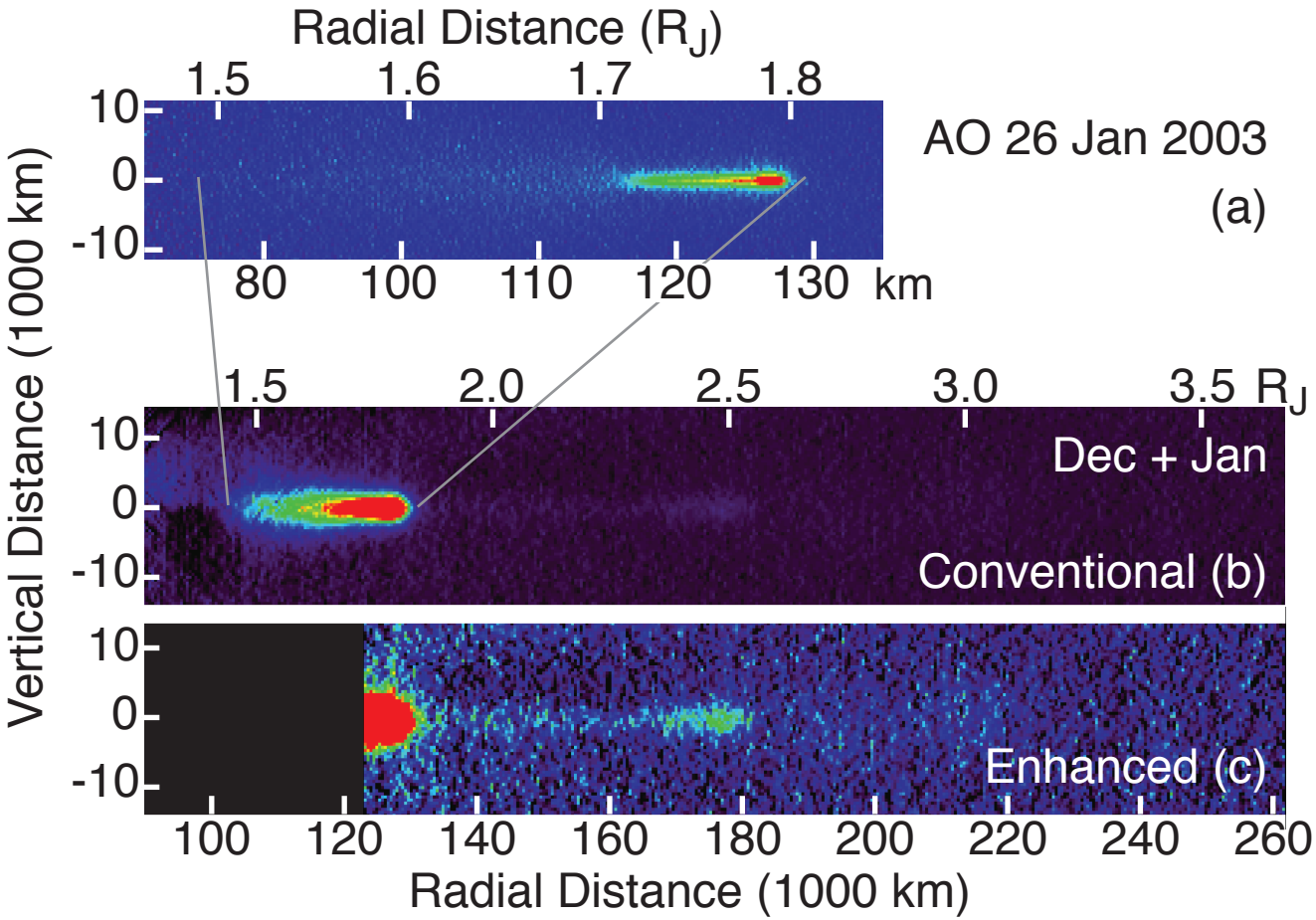
Radial Distance ($R_J$)
1.5
1.6
1.7
1.8
10
0
-10
80
100
110
120
130
km
AO 26 Jan 2003
(a)
1.5
2.0
2.5
3.0
3.5 $R_J$
Dec + Jan
Conventional (b)
Enhanced (c)
Vertical Distance (1000 km)
100
120
140
160
180
200
220
240
260
Radial Distance (1000 km)

Fig. 3

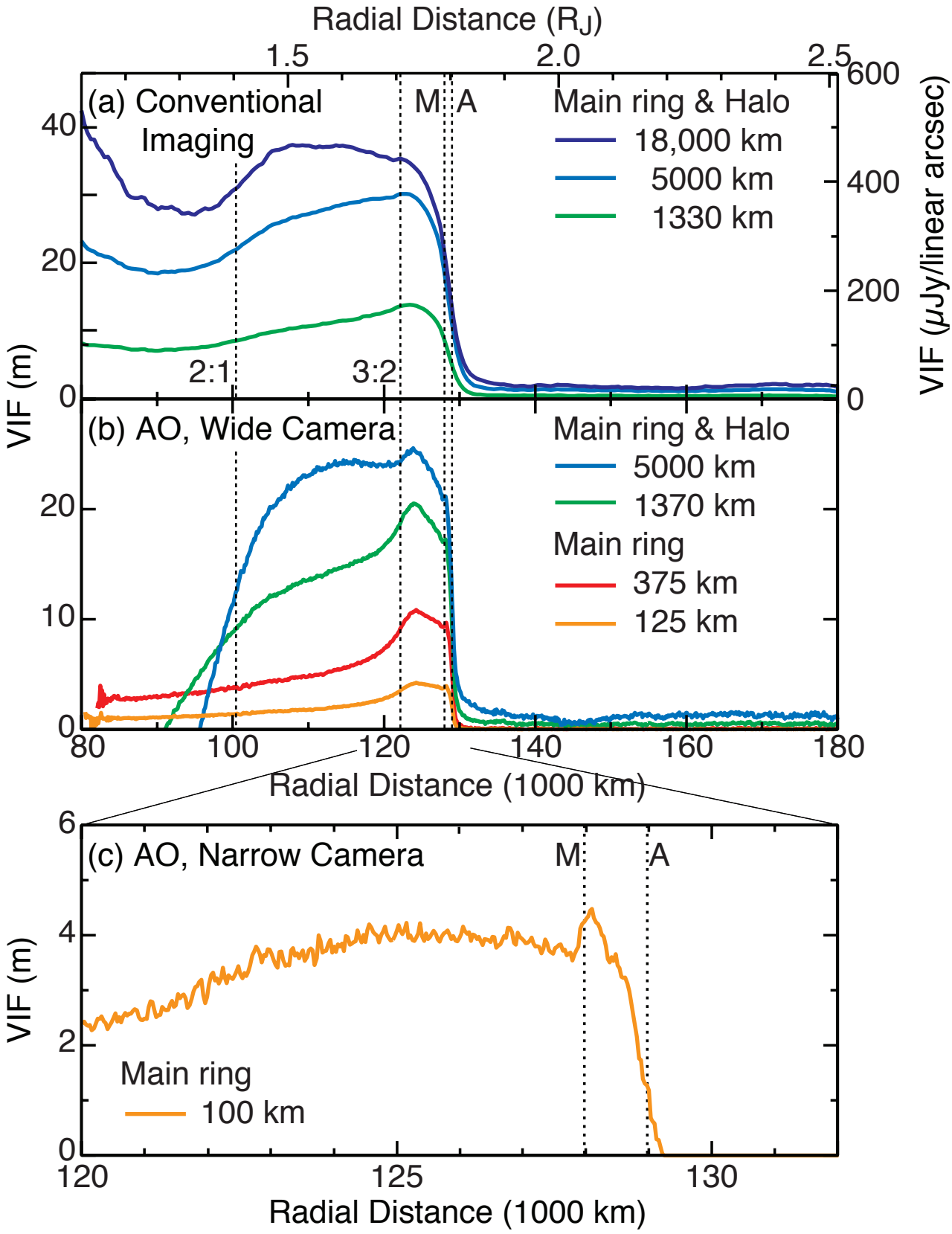
Radial Distance ($R_J$)
1.5
2.0
2.5
(a) Conventional Imaging
M
A
Main ring & Halo
18,000 km
5000 km
1330 km
2:1
3:2
VIF (m)
VIF (μJy/linear arcsec)
(b) AO, Wide Camera
Main ring & Halo
5000 km
1370 km
Main ring
375 km
125 km
Radial Distance (1000 km)
(c) AO, Narrow Camera
Main ring
100 km
Radial Distance (1000 km)

Fig. 4

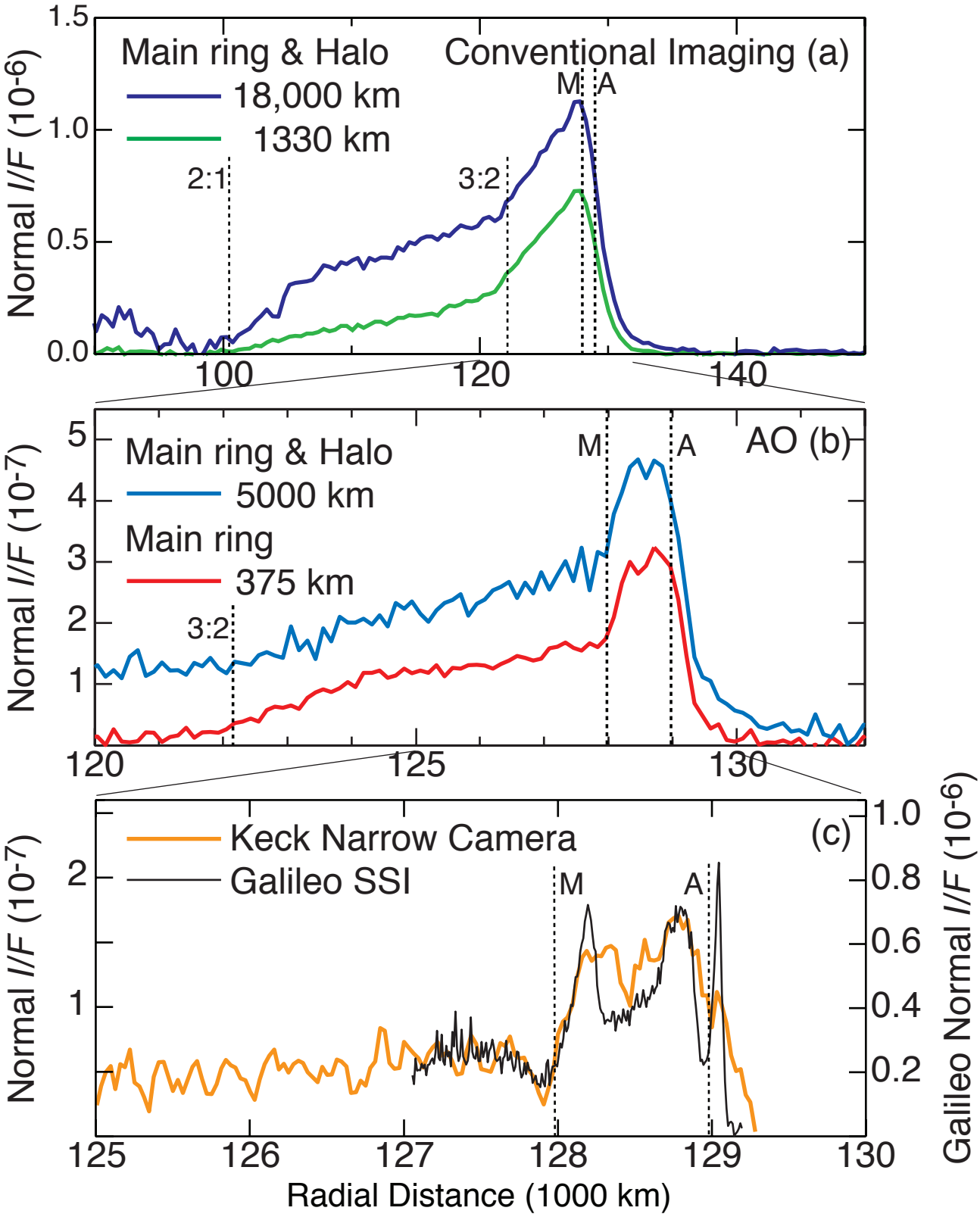
Main ring & Halo
18,000 km
1330 km
Conventional Imaging (a)
M
A
2:1
3:2
Normal I/F (10-6)
1.5
1.0
0.5
0.0
100
120
140
Main ring & Halo
5000 km
Main ring
375 km
3:2
M
A
AO (b)
Normal I/F (10-7)
5
4
3
2
1
120
125
130
Keck Narrow Camera
Galileo SSI
(c)
M
A
Normal I/F (10-7)
2
1
Galileo Normal I/F (10-6)
1.0
0.8
0.6
0.4
0.2
125
126
127
128
129
130
Radial Distance (1000 km)

Fig. 5

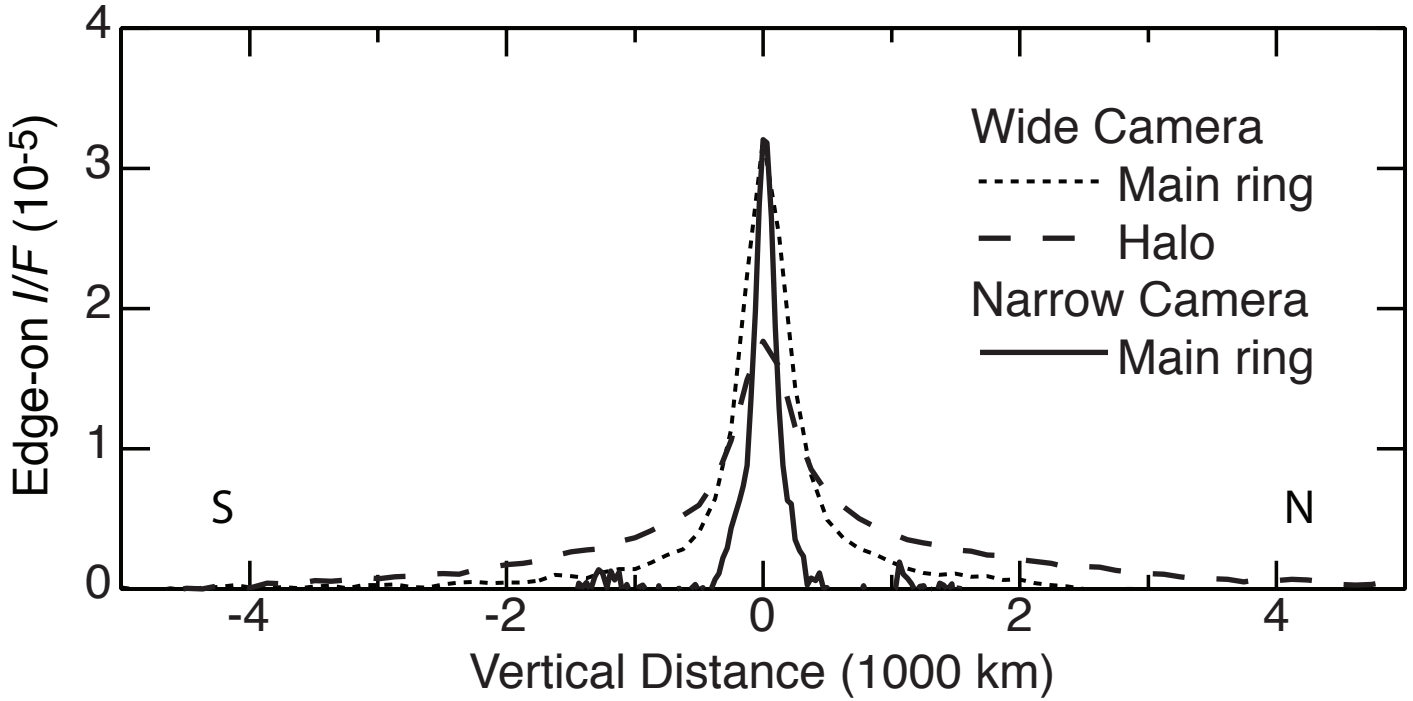
Edge-on I/F (10-5)
4
3
2
1
0
-4
-2
0
2
4
Vertical Distance (1000 km)
S
N
Wide Camera
Main ring
Halo
Narrow Camera
Main ring

Fig. 6

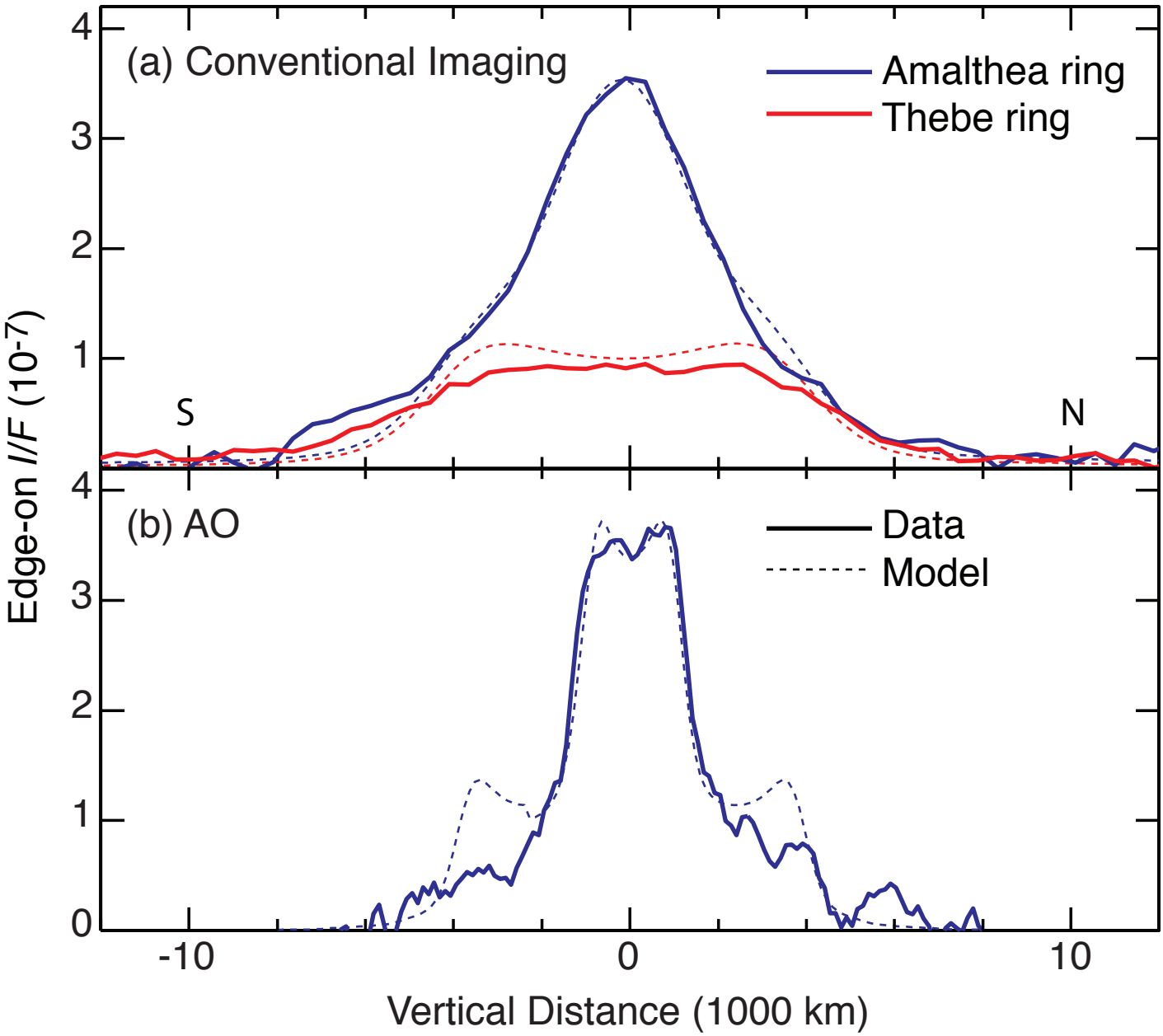
(a) Conventional Imaging
Amalthea ring
Thebe ring
S
N
(b) AO
Data
Model
Edge-on I/F (10-7)
Vertical Distance (1000 km)
4
3
2
1
0
-10
0
10

Fig. 7

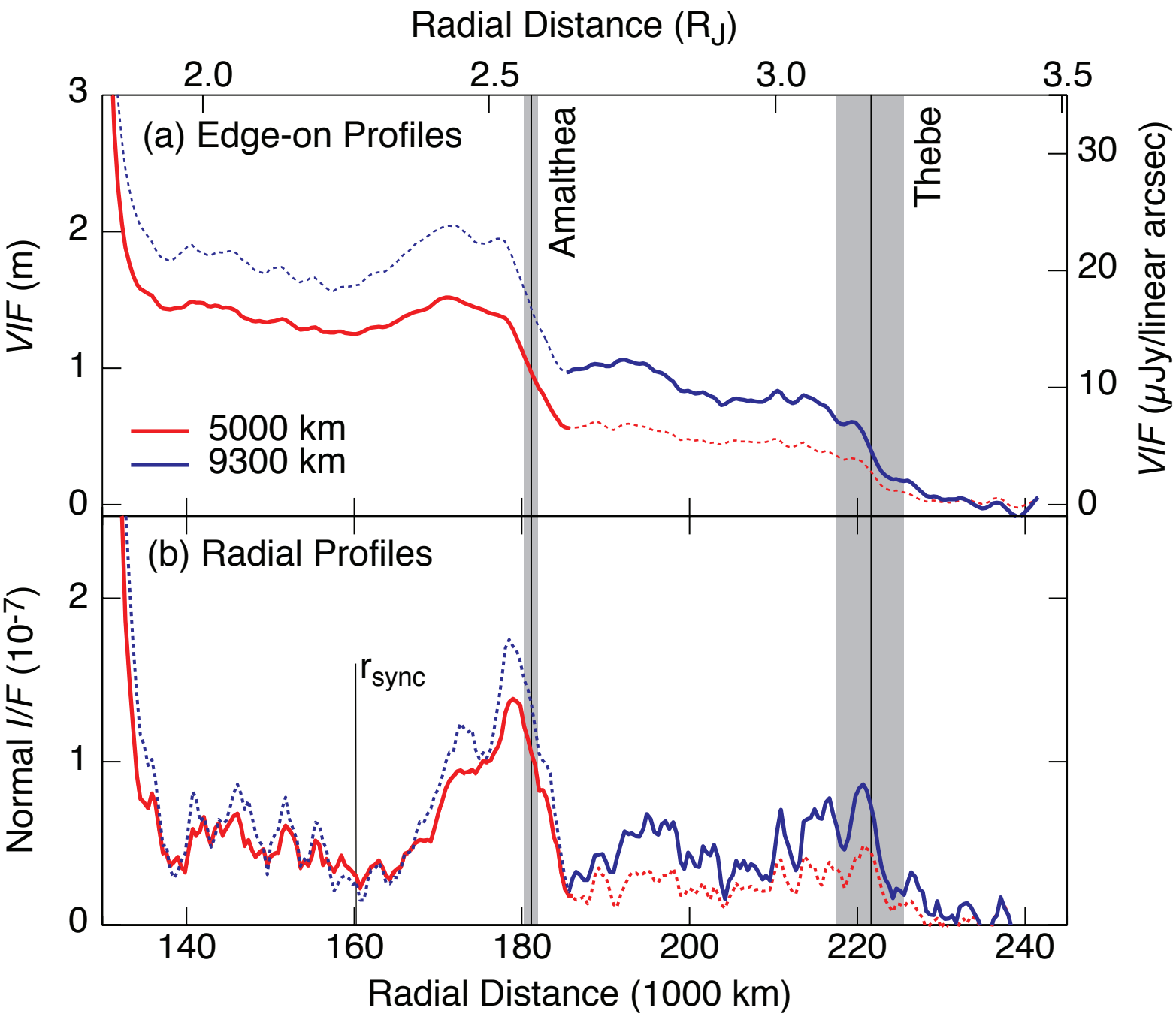
Radial Distance ($R_J$)
2.0
2.5
3.0
3.5
(a) Edge-on Profiles
Amalthea
Thebe
5000 km
9300 km
*I/F* (m)
*I/F* (μJy/linear arcsec)
(b) Radial Profiles
$r_{sync}$
Normal *I/F* ($10^{-7}$)
140
160
180
200
220
240
Radial Distance (1000 km)

Fig. 8